Journal of Power Sources 193 (2009) 602–606

Contents lists available at ScienceDirect

Journal of Power Sources

journal homepage: www.elsevier.com/locate/jpowsour

Short communication

Electrochemical performance of a glucose/oxygen microfluidic biofuel cell

A. Zebda[a], L. Renaud[b,c], M. Cretin[a], C. Innocent[a], F. Pichot[d], R. Ferrigno[b,c], S. Tingry[a,*]

[a] Institut Européen des Membranes, UMR 5635, ENSCM-UMII-CNRS, place Eugène Bataillon, 34095 Montpellier, France
[b] Institut des Nanotechnologies de Lyon, INL, CNRS UMR5270, Université de Lyon, F-69003 Lyon, France
[c] Université Lyon 1, Villeurbanne F-69622, France
[d] Centrale de Technologies en Micro et Nanoélectronique, Université Montpellier 2, place Eugène Bataillon, 34095 Montpellier, France

ARTICLE INFO

Article history:
Received 9 February 2009
Received in revised form 20 April 2009
Accepted 26 April 2009
Available online 3 May 2009

Keywords:
Biofuel cell
Enzymes
Laminar flow
Microfluidics

ABSTRACT

A microfluidic glucose/O_2 biofuel cell, delivering electrical power, is developed based on both laminar flow and biological enzyme strategies. The device consists of a Y-shaped microfluidic channel in which fuel and oxidant streams flow laminarly in parallel at gold electrode surfaces without convective mixing. At the anode, the glucose is oxidized by the enzyme glucose oxidase whereas at the cathode, the oxygen is reduced by the enzyme laccase, in the presence of specific redox mediators. Such cell design protects the anode from interfering parasite reaction of O_2 at the anode and works with different streams of oxidant and fuel for optimal operation of the enzymes. The dependence of the flow rate on the current is evaluated in order to determine the optimum flow that would provide little to no mixing while yielding high current densities. The maximum power density delivered by the assembled biofuel cell reaches 110 $\mu W\,cm^{-2}$ at 0.3 V with 10 mM glucose at 23 °C. This research demonstrates the feasibility of advanced microfabrication techniques to build an efficient microfluidic glucose/O_2 biofuel cell device.

1. Introduction

Enzymatic Biofuel Cells (BFC) convert chemical energy into electrical energy *via* specific enzymes as catalysts. Biofuel cells are strong candidates to supply power for miniature portable electronic or biomedical devices. Indeed, renewable energies (biofuels) and enzymes constitute interesting sustainable sources for greatly limiting environmental impact and having a strong growth in market share. A recent trend in the development of biofuel cells working with enzymes is the use of glucose as fuel and O_2 as oxidant [1,2]. Glucose is electrooxidized to gluconolactone by the enzyme glucose oxidase (GOD) at the anode and dioxygen is reduced to water at the cathode by the specific enzymes such as laccase or bilirubin oxidase. Redox mediators are usually introduced in the system to mediate electron transfer from the biocatalytic active sites to the electrodes.

However, although dissolved O_2 reacts with the cathodic enzyme, it also acts as interfering substance for anode reactions: O_2 intercepts electrons from the anode by reacting with GOD and consequently lower the electron flow and the delivered power. Such phenomenon was reported by the decreases of the power density of 30% [3] and 50% [4] for biofuel cells in O_2-saturated solution compared to air-saturated solution because of the undesirable electron transfer from GOD to the dissolved O_2. To decrease the O_2 flux to the bioanode, strategies have been developed based on the physical design of the devices by using a separator between anode and cathode electrodes [5] or compartmentalized porous electrodes [4]. However, these systems are not suitable to miniature power sources.

To develop power supply for portable electronics, microfluidic fuel cells working from hydrogen, methanol or formic acid as fuel have recently attracted significant attention [6–9]. These systems exploit the laminar flow of fluids in microchannel at low Reynolds number that contribute to limit convective mixing [10–12]. In such devices, streams of fuel and oxidant flow in parallel within the microchannel without needing a membrane to minimize the ohmic drop and then maximize the current density. Protons diffuse through the liquid–liquid interface created by the contacting streams of fuel and oxidant. The electrochemical reactions take place at the anode and cathode located within the respective streams. The performances of the devices are evaluated from voltage, current density and delivered power density. As summarized by authors [11,13], the two processes that determine the performance of microfluidic fuel cells are (i) cross-diffusional mixing of fuel and oxidant at the interface between the two streams and (ii) the formation of depletion boundary layers at the surface of the electrodes as the result of the reaction of fuel and oxidant. Interesting papers have presented theoretical and experimental works to describe the role of flow rate, microchannel geometry, and

* Corresponding author. Fax: +33 4 67 14 91 19.
E-mail address: sophie.tingry@iemm.univ-montp2.fr (S. Tingry).

0378-7753/$ – see front matter © 2009 Elsevier B.V. All rights reserved.
doi:10.1016/j.jpowsour.2009.04.066

location of electrodes within microfluidic systems on their performance [13–16].

Similarly to microfluidic fuel cells, advanced microfabrication techniques can be applied to build components of microfluidic enzymatic biofuel cells. As described earlier, microfluidic enzyme biofuel cells have been developed based on both laminar flow within a microchannel and biological enzyme strategies. Palmore and co-workers [17,18] have developed a microfluidic fuel cell working from the direct oxidation of 2,2′-azinobis (3-ethylbenzothiazoline-6-sulfonate) (ABTS) at the anode, and the reduction of ABTS by the enzyme laccase at the cathode. A transport model was developed to describe the optimal conditions for maximizing both the average current density and the percentage of fuel utilized. The maximum power density of the device was enhanced by 25% by designing the suitable length and spacing of the electrodes within the microchannel. Another enzyme-based microfluidic biofuel cell has been developed that generated electric power from glucose oxidation with an anode coated by immobilized glucose deshydrogenase and a bilirubin oxidase-adsorbed O_2 cathode [19]. The originality of the work was the electrode-arrangement in a single flow channel. Dissolved O_2 was pre-reduced at an upstream cathode to protect the downstream anode from oxidative environment. The maximum cell current was increased by 10% with this cell configuration.

In this paper, we describe a glucose/O_2 biofuel cell based on a Y-shaped microfluidic channel to deliver electrical current. The objective is to exploit the laminar flow of the streams to protect the anode from interfering parasite reactions of O_2 and to use different media for optimal operation of the enzymes. The dimensions and operating conditions of the microfluidic device were such that fluid flow was pressure driven and characterized by a Reynolds number less than 2000. At the anode, the glucose was oxidized by the enzyme GOD in presence of the redox mediator hexacyanoferrate ($Fe(CN)_6^{3-}$), whereas at the cathode, the oxygen was reduced by the enzyme laccase in presence of the redox mediator ABTS. Electrochemical characterizations of the device were performed as a function of the flow rate of the streams through the microchannel. The device was evaluated for its use as a functional glucose/O_2 biofuel cell to generate maximum power density.

2. Experimental

2.1. Chemicals

ABTS, hexacyanoferrate, GOD from Aspergillus Niger (198 000 U mg^{-1} solid) and laccase from Trametes Versicolor (20 U mg^{-1} solid) were purchased from Sigma–Aldrich and used without further purification. Buffers were prepared with sodium dihydrogen phosphate monohydrate ($NaH_2PO_4{\cdot}H_2O$) and disodium hydrogen phosphate (Na_2HPO_4) salts (pH 7.0) from Merck, and with citric acid (Prolabo) and $NaH_2PO_4{\cdot}H_2O$ salt (pH 3.0). β-D-Glucose was from Prolabo and was prepared in phosphate buffer 0.1 M pH 7.0 at least 24 h before its use. Aqueous solutions were prepared using 18.2 MΩ cm MilliQ water (Millipore).

2.2. Fabrication of microchannel

The microfluidic chip was fabricated using a two-part poly(dimethylsiloxane) (PDMS) elastomer and a standard soft lithography method. Firstly, a master was obtained using an Etectec HQ-6100 negative dry film photoresist, as published elsewhere [20]. Typically, a glass slide was preliminary cleaned, modified by a 35 μm Etertec HQ-6100 first film layer and exposed to UV light. Two photoresist layers of 35 μm thickness were then sequentially laminated on the firstly exposed layer. After exposition to UV light through a photomask, the structure was then developed by spraying an aqueous solution of sodium carbonate (1 wt%) during 4 min. The structure was hardened by a second irradiation. The master was then replicated in PDMS [21] at 70 °C during 2 h. After cooling, the PDMS slab was peeled off from the master and holes were punched using a 1.2 mm diameter tube, to provide an access for Teflon tubing. The PDMS slab was then aligned with a glass slide containing electrodes. The device consisted of a Y-shaped channel in PDMS with two inlets and two outlets (Fig. 1). The microchannel dimensions were: L = 25 mm, w = 2 mm and h = 75 μm.

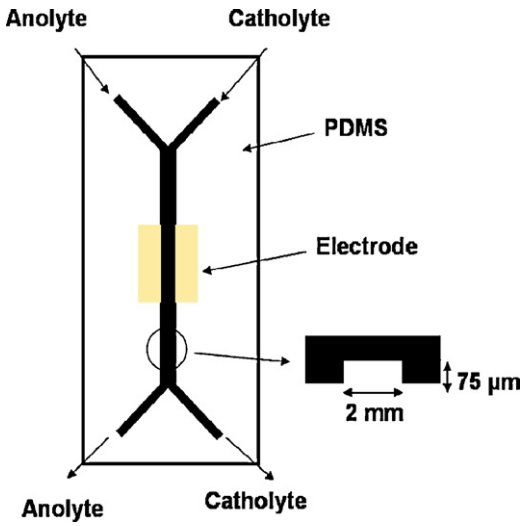

Fig. 1. Scheme of the glucose/O_2 biofuel cell consisted in a Y-shaped microfluidic channel in PDMS with two inlets and two outlets.

2.3. Microfluidic cell and electrochemical measurements

The gold electrodes (10 mm length and 2 mm wide) were deposited by sputtering on a glass substrate (Au: 300 nm thick on a 10 nm thick Cr adhesion layer). The separation between the cathode and the anode was 1 mm.

The catholyte solution consisted of laccase (0.5 mg mL^{-1}) and ABTS (5 mM) in 0.2 M citrate buffer at pH 3, saturated with oxygen. The anolyte consisted of GOD (0.5 mg mL^{-1}) and $Fe(CN)_6^{3-}$ (10 mM) in 0.2 M phosphate buffer at pH 7, purged with nitrogen gas. A syringe pump (Harvad) was used to pump the solutions into the microchannel at a flow rate varying from 0.1 to 1 mL min^{-1}.

The electrochemical measurements were performed using a potentiostat Autolab (Eco chemie) connected to a computer. The fuel cell performance was evaluated at 23 °C by measuring the cell voltage while varying the current density.

2.4. Numerical simulations

In the microchannel, the profile of the flow rate was obtained by solving numerically the Navier–Stokes equations:

$$\frac{\partial^2 U}{\partial y^2} = \frac{1}{\eta}\frac{\Delta P}{L} \quad (1)$$

where U is the fluid velocity along the x direction, η is the dynamic viscosity of the buffer (assuming the same as water), ΔP is the pressure-drop between inlet and outlet and L is the length of the simulated microchannel. The boundary conditions were chosen as following: no-slip at the walls and at the electrodes, and ΔP adapted to the hydrodynamic resistance of the microchannel [22] (ΔP = 236 Pa for a 100 μL min^{-1} flow).

We chose a 2D approach, due to the very large aspect ratio of the cross-section of the microchannel (75 μm height and 2000 μm width), leading to a pseudo infinite-plate flow (steady-state analy-

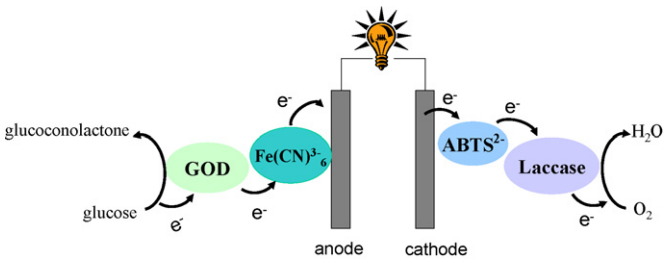

Fig. 2. Electron transfer steps at the biocathode and the bioanode.

sis). The directions along the length and height of the microchannel were indicated as x and y coordinates, respectively. A typical parabolic rate profile was obtained in agreement with analytical solution of this problem.

In the microchannel, we determined the profile of the depletion zone attributed to the lowest diffusing redox mediator, ABTS ($D = 0.45\ 10^{-9}\ m^2\ s^{-1}$ [23]) by solving numerically the convection–diffusion Eq. (2) on FEMLAB 3.1 multiphysics software. The boundary conditions were chosen as following: $C = C_0$ at the inlet, "no reaction" at the upper wall, and $C = 0$ at the electrode (instantaneous reaction at the electrode).

$$U\frac{\partial C}{\partial x} = D\left(\frac{\partial^2 C}{\partial x^2} + \frac{\partial^2 C}{\partial y^2}\right) \quad (2)$$

During multistream laminar flow, the diffusion transverse to the direction of flow results in the mixing of the two streams. The broadening of the mixing layer at a planar electrode surface, δ_{mix}, was given by Eq. (3) [24]:

$$\delta_{mix} = \left(\frac{Dhx}{U_{av}}\right)^{1/3} \quad (3)$$

where D is the species diffusivity, h the channel height, x the downstream distance, U_{av} the average velocity ($m\ s^{-1}$) ($U_{av} = Q/s$ with Q the flow rate and $s = 1/2wh$ the microchannel section).

3. Results and discussion

3.1. Physicochemical analysis

The redox reactions in the BFC are the electro-oxidation of glucose in gluconolactone at the anode by the glucose oxidase with $Fe(CN)_6^{3-}$, and the electro-reduction of dioxygen in water at the cathode by the laccase with ABTS (Fig. 2). The mediators $Fe(CN)_6^{3-}/Fe(CN)_6^{4-}$ ($E'^\circ = 0.12$ V *vs* SCE) and $ABTS^{\bullet-}$/ABTS ($E'^\circ = 0.4$ V *vs* SCE) have been chosen with a formal potential close to that of GOD ($E'^\circ = -0.34$ V *vs* SCE for Aspergillus Niger [25]) and laccase ($E'^\circ = 0.535$ V *vs* SCE for Trametes Versicolor [26]), respectively.

The microfluidic biofuel cell exploits the laminar flow of fluids in the microchannel at low Reynolds number $Re = U_{av}D_h/\nu$ (with D_h is the hydraulic diameter = 2 h, ν the kinematic viscosity of water $10^{-6}\ m^2\ s^{-1}$), that contributes to limit convective mixing [12]. For flow rates in the range 100–1000 $\mu L\ min^{-1}$, the Reynolds number varies between 3.33 and 33.3. In such conditions, the mass transport is achieved by both diffusion and convection transport. The ratio of diffusive to convective time scales is denoted as the Peclet number Pe ($Pe = U_{av}h/D$) [27]. For low Peclet numbers ($\ll 1$), diffusion dominates and it is the main transport regime. On the other hand for high Peclet numbers ($\gg 1$), convection dominates. In our case, the Pe number varies from 3700 to 37 000 for a flow rate in the range 100–1000 $\mu L\ min^{-1}$, for the lowest diffusing redox mediator ABTS, and the diffusive transport along the microchannel can be thus neglected.

To check the possibility that diffusive crossover contributes to the loss of current, we calculated the width of the mixed region δ_{mix} using Eq. (3). For a 1-cm-electrode length and the lower flow rate 100 $\mu L\ min^{-1}$, δ_{mix} was 24.8 μm. As the electrodes are separated by 1 mm, diffusive crossover does not decrease the performance of the fuel cell.

Rapid transport of reactants to the electrodes is essential to provide high power densities. When a heterogeneous reaction occurs at electrode surface, depletion of the reactant results in formation of a depletion zone near the electrode surface where lower conversion rates occur as the reactant concentration is lower than in the bulk region. Under convective flow conditions, the thickness of the depletion zone at the surface of the electrode is a function of the distance from the inlet edge. As shown by simulated concentration profiles (Fig. 3) evaluated from Eq. (2), during the operation of the biofuel cell, depletion zones at the inlet and outlet cross-sections of the microchannel are created near the surface of the electrode (length 1 cm). The concentration of ABTS decreases next to the surface along the electrode. The current density decreases because of the concomitant increase of the depletion zone. The thickness of the depletion layer in outlet of the electrode is 37 μm for a flow rate 100 $\mu L\ min^{-1}$ and 17 μm for 1000 $\mu L\ min^{-1}$.

3.2. Influence of the flow rate

The performance of the microfluidic system can be affected by the flow rate of the streams, which regulates the depletion layer thickness. Fig. 4 shows the polarization curves of the biofuel cell as a function of the flow rate. The flow rate varies depending on geometry and composition/concentration of fuel and oxidant streams. The optimum flow rate would, therefore, provide little to no fuel crossover while yielding high reactants consumption. In our operating conditions, maximal current densities increase with flow rate from 0.35 to 0.69 $mA\ cm^{-2}$. The open circuit voltage (OCV) of the device varies slightly between 0.52 and 0.55 V. The impact of mass transport limitations, from the bulk solution to the electrode surface, is thus reduced by enhanced convective transport at high flow rates. The polarization curves at high flow rate (700 $\mu L\ min^{-1}$ and 1000 $\mu L\ min^{-1}$) separate only at high current densities, which indicates that the mass transport predominates in this current range.

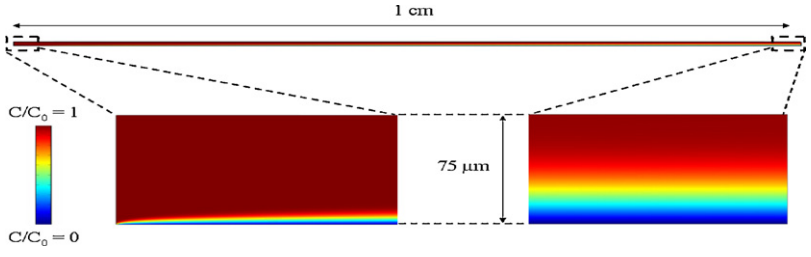

Fig. 3. 2D profile of ABTS concentration in the microchannel at the inlet and outlet cross-sections (along 150 μm of the electrode). Depletion zones are generated as ABTS is consumed in the proximity of the electrode.

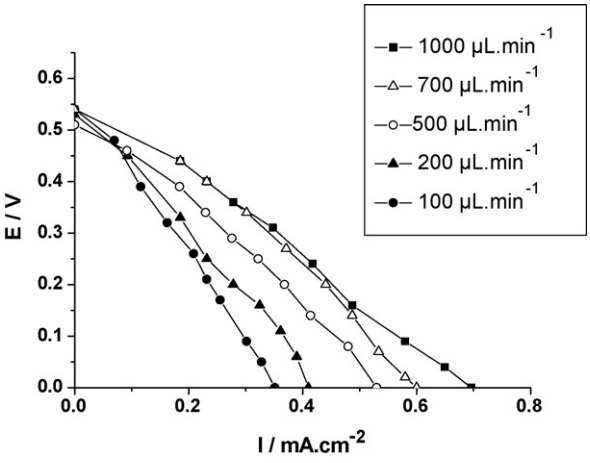

Fig. 4. Polarization curves of the microfluidic glucose/O_2 biofuel cell at different flow rates.

Based on the experiments, an operating flow rate of 1000 µL min^{-1} was chosen to evaluate the performance of the biofuel cell.

In a regime controlled by convective transport, the maximal current density varies as linearly with the cubic root of flow rate as supported by the well-known Levich Eq. (4):

$$I_{max} = 0.925nFLC^{\circ}(wD)^{2/3}(4U_{av}/h)^{1/3} \quad (4)$$

where n is the number of electron exchanged, F is the Faraday constant, C° is the ABTS concentration, w and h are the width and the height of the channel and u_{av} is the average rate (ratio of the flow rate to the microchannel section).

In our case, the calculated values of normalized current density (I) obtained experimentally vary linearly with the cubic root of flow rate (Q) (Fig. 5). This result confirms thus that the current is limited by convection transport. Based on numerical simulations (from Eqs. (1) and (2)), the simulated values of normalized current density (I) closely match the experimental data.

3.3. Performance of the microfluidic biofuel cell

Fig. 6 presents the power density at 1000 µL min^{-1} using the oxidant stream saturated with oxygen at pH 3 and the fuel stream purged with nitrogen gas at pH 7. The maximum power density delivered by the biofuel cell is 110 µW cm^{-2} at 0.3 V at 23 °C. This value is higher than previous reported values of 64 µW cm^{-2} at

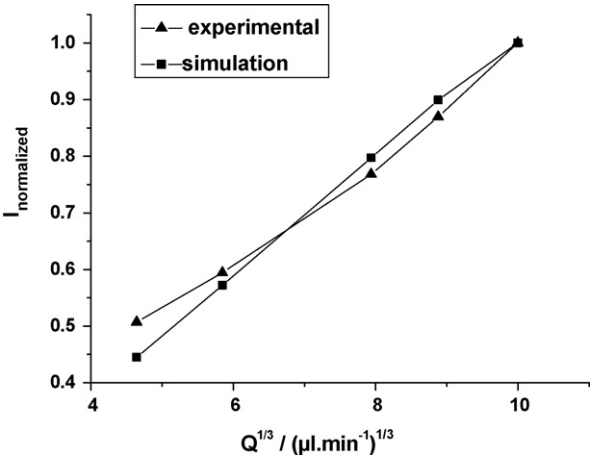

Fig. 5. Normalized maximum current density (I) as a function of the cubic root of flow rate (Q) for a glucose/O_2 microfluidic biofuel cell.

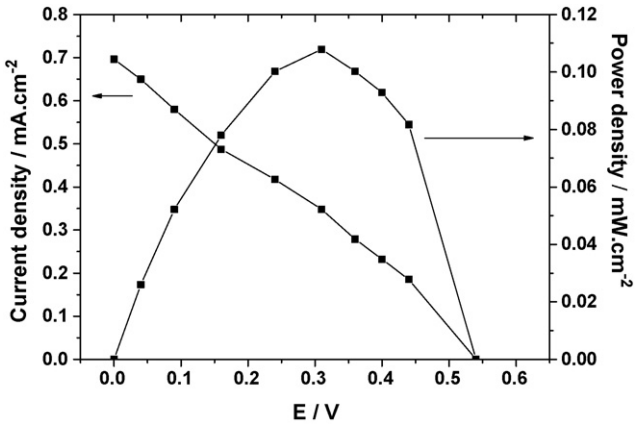

Fig. 6. Power density *vs* voltage plot generated from the microfluidic glucose/O_2 biofuel cell, at 23 °C at 1000 µL min^{-1}.

0.4 V at 23 °C for a miniaturized glucose biofuel cell with immobilized enzymes [28], and of 26 µW cm^{-2} at 0.15 V at 23 °C [17].

From the performance of the fuel cell, the fill factor (defined as the ratio of the actual maximum obtained power to the theoretical power) is approximately 28% based on a maximum power density of 110 µW cm^{-2}, an OCV of 0.55 V and a short-circuit current of 690 µW cm^{-2}. This value is twice higher than the one reported for a microfluidic biofuel cell [17] that used only one enzyme (laccase) in the catholyte stream. This observation suggests that the use of two enzymes, both in the catholyte and the anolyte stream, improves the biofuel cell performance.

3.4. Optimization of electrode length by numerical simulations

For electrochemical reactions under laminar flow, the thickness of the depletion boundary layer is not constant and increases along the electrode leading to a decrease in current density. One way to reduce depletion layer limitation and to maximize the current density, is to reduce the electrode length. Simulations were exploited to optimize the electrode length corresponding to the maximum current density. We calculated the diffusive flux at the electrode, defined as:

$$J_{diff}(x) = D\left.\frac{\partial C}{\partial y}\right|_{electrode} \quad (5)$$

And, therefore, the total current is expressed as:

$$I_{tot} = \int_{electrode} nFJ_{diff}(x)\,dx = nFD\int_{electrode}\left(\left.\frac{\partial C}{\partial y}\right|_{y=0}\right)dx \quad (6)$$

where n is the number of electrons exchanged, and F is the Faraday constant.

Fig. 7 shows for different flow rates the evolution of J_{diff} along the electrode. Between 0 and 1 mm, J_{diff} decreases dramatically from 1.8 to 0.35 mol m^{-2} s^{-1} and slowly between 1 and 10 mm. It shows that the depletion layer effect is more significant at the upstream of the microchannel.

Using Eq. (6), we calculated the variation of current density between 1 and 10 mm. It was found that whatever the flow rate, the current density at 1 mm was four times higher than at 10 mm. These results suggest that the performance of microfluidic cell should be better for shorter electrodes. This is in agreement with the work described by Palmore and co-workers [18]. However, by limiting the electrode surface, the power delivered may be limited. To resolve this problem, we are currently working on the optimization of a microchannel based on multi-entries with short electrodes.

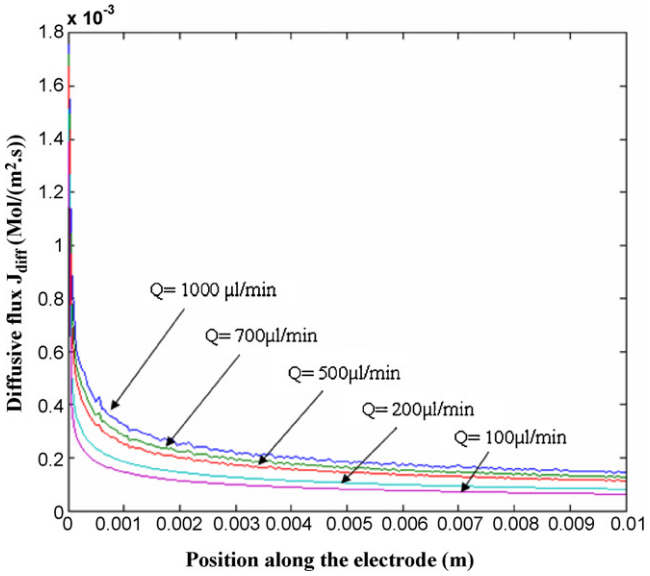

Fig. 7. Diffusive flux (J_{diff}) along the electrode (1 cm length) for 5 different flow rates Q (C_{ABTS} = 5 mM).

4. Conclusion

This work has demonstrated the feasibility of a microfluidic glucose/O_2 BFC to operate by taking into account laminar flow. Streams of fuel and oxidant flow laminarly in parallel at gold electrode surfaces without convective mixing. The goal was to design an efficient device that protects the anode from interfering parasite reaction of O_2 at the anode and works with different streams of oxidant and fuel for optimal operation of the enzymes.

Experimental and theoretical results have shown that the performance of the biofuel cell is limited by the transport of reactants through the depletion layer along the electrode surface. Improvements have been realized by enhancement of the convective transport of reactants in the microchannel at an optimum flow rate. The current density was increased to 0.69 mA cm^{-2}. The maximum of power density delivered by the assembled biofuel cell reached 110 μW cm^{-2} at 0.3 V with 10 mM glucose at 23 °C. Numerical simulations demonstrated that the use of shorter electrodes decreased the depletion layer limitation, but decreased at the same time electrode surface and consequently the delivered power.

This research demonstrates the feasibility of advanced microfabrication techniques to build efficient microfluidic glucose/O_2 biofuel cell device compared to standard miniaturized glucose biofuel cell.

Acknowledgment

This work was supported by a CNRS postdoctoral fellowship.

References

[1] K. Kendall, Nat. Mater. 1 (2002) 211–212.
[2] F. Robert, Science 296 (2002) 1222–1224.
[3] H.H. Kim, N. Mano, X.C. Zhang, A. Heller, J. Electrochem. Soc. 150 (2003) A209–A213.
[4] L. Brunel, J. Denele, K. Servat, K.B. Kokoh, C. Jolivalt, C. Innocent, M. Cretin, M. Rolland, S. Tingry, Electrochem. Commun. 9 (2007) 331–336.
[5] S. Tsujimura, M. Fujita, H. Tatsumi, K. Kano, T. Ikeda, Phys. Chem. Chem. Phys. 3 (2001) 1331–1335.
[6] A. Bazylak, D. Sinton, N. Djilali, J. Power Sources 143 (2005) 57–66.
[7] R.S. Jayashree, L. Gancs, E.R. Choban, A. Primak, D. Natarajan, L.J. Markoski, P.J.A. Kenis, J. Am. Chem. Soc. 127 (2005) 16758–16759.
[8] C.M. Moore, S.D. Minteer, R.S. Martin, Lab Chip 5 (2005) 218–225.
[9] J.L. Cohen, D.A. Westly, A. Pechenik, H.D. Abruna, J. Power Sources 139 (2005) 96–105.
[10] R. Ferrigno, A.D. Stroock, T.D. Clark, M. Mayer, G.M. Whitesides, J. Am. Chem. Soc. 124 (2002) 12930–12931.
[11] T.J.M. Luo, J.F. Fei, K.G. Lim, G.T.M. Palmore, Membraneless fuel cells: an application of microfluidics, in: ACS Symposium Series 890, 2005.
[12] E.R. Choban, L.J. Markoski, A. Wieckowski, P.J.A. Kenis, J. Power Sources 128 (2004) 54–60.
[13] M.H. Sun, G.V. Casquillas, S.S. Guo, J. Shi, H. Ji, Q. Ouyang, Y. Chen, Microelectron. Eng. 84 (2007) 1182–1185.
[14] C. Amatore, N. Da Mota, C. Della, L. Thouin, Anal. Chem. 79 (2007) 8502–8510.
[15] F. Chen, M.H. Chang, M.K. Lin, Electrochim. Acta 52 (2007) 2506–2514.
[16] E.R. Choban, P. Waszczuk, P.J.A. Kenis, Electrochem. Solid-State Lett. 8 (2005) A348–A352.
[17] K.G. Lim, G. Tayhas, R. Palmore, Biosens. Bioelectron. 22 (2007) 941–947.
[18] J. Lee, K.G. Lim, G. Tayhas, R. Palmore, A. Tripathi, Anal. Chem. 79 (2007) 7301–7307.
[19] M. Togo, A. Takamura, T. Asai, H. Kaji, M. Nishizawa, J. Power Sources 178 (2008) 53–58.
[20] K. Stephan, P. Pittet, L. Renaud, P. Kleimann, P. Morin, N. Ouaini, R. Ferrigno, J. Micromech. Microeng. 17 (2007) N69–N74.
[21] D.C. Duffy, J.C. McDonald, O.J.A. Schueller, G.M. Whitesides, Anal. Chem. 70 (1998) 4974–4984.
[22] L. Renaud, C. Malhaire, P. Kleimann, D. Barbier, P. Morin, Mater. Sci. Eng. C 28 (2008) 910–917.
[23] G.T.R. Palmore, H.H. Kim, J. Electroanal. Chem. 464 (1999) 110–117.
[24] R.F. Ismagilov, A.D. Stroock, P.J.A. Kenis, G. Whitesides, H.A. Stone, Appl. Phys. Lett. 76 (2000) 2376–2378.
[25] M.T. Stankovitch, L.M. Schopfer, V.J. Massey, J. Biol. Chem. 253 (1978) 4971–4979.
[26] E.I. Solomon, U.M. Sundaram, T.E. Machonkin, Chem. Rev. 96 (1996) 2563–2606.
[27] R.B. Bird, W.E. Stewart, E.N. Lightfoot, Transport Phenomena, Wiley, New York, 2001.
[28] T. Chen, S.C. Barton, G. Binyamin, Z. Gao, Y. Zhang, H.H. Kim, A. Heller, J. Am. Chem. Soc. 123 (2001) 8630–8631.